Developing Numerical Tools to Improve the Diagnosis of Peripheral Artery Disease

L. J. Barratt*[1,2], Y. Somani[3], Al Benson[3], T. Lassila[2], and M. Bailey[4]

[1]EPSRC CDT in Future Fluid Dynamics
[2]School of Computer Science, University of Leeds, LS2 9JT
[3]School of Biomedical Sciences, University of Leeds, LS2 9JT
[4]Schools of Medicine, University of Leeds, LS2 9JT

September 1, 2025

1 Introduction

Peripheral artery disease (PAD) affects greater than 10% of adults aged 65+ (Houghton et al., 2024) and is caused by atherosclerotic narrowing of peripheral arteries, reducing muscle oxygen delivery and triggering exercise-induced pain (Fowkes et al., 2013). PAD doubles cardiovascular event risk (Sprenger et al., 2021), yet traditional diagnostic methods often miss cases – particularly in patients with calcified arteries, dysfunction of the microcirculation, and other atypical presentations (more frequent in women), leading to delayed treatment and worse outcomes (Pabon et al., 2022).

This project will explore the interaction of the key biological systems (blood delivery, vascular function, and oxygen uptake) degraded in PAD patients that are not captured in current diagnostic methods; therefore, making way for improved detection of PAD.

2 Model Overview

2.1 Model of Macrocirculation

Blood flow in the large arteries is described using 1D Navier–Stokes for flow in compliant tubes (Alastruey, K. H. Parker, et al., 2008; Alastruey, Kim H. Parker, et al., 2012). The continuity and momentum equations are formed as follows,

$$\frac{\partial A}{\partial t} + \frac{\partial Au}{\partial x} = 0, \tag{1}$$

$$\frac{\partial u}{\partial t} + \alpha u \frac{\partial u}{\partial x} + \frac{1}{\rho}\frac{\partial p}{\partial x} + \frac{2\pi\mu(\gamma+2)u}{\rho A} = 0. \tag{2}$$

where x is the axial direction, $A = A(x,t)$ is the cross-sectional area, $u = u(x,t)$ is the section-averaged velocity, $p = p(x,t)$ is the internal pressure, ρ is the constant blood density, μ is the

*Corresponding author: scljb@leeds.ac.uk

constant blood viscosity, γ is a parameter describing the velocity profile, and α is the momentum correction coefficient, where $\alpha = \gamma + 2\gamma + 1$. The fourth term of Equation **??** represents viscous forces in the fluid dependent on the assumed velocity profile. In this work, the profile is assumed constant and takes the form presented in Chapter **??**,

$$\hat{u}(r) = \frac{\gamma + 2}{\gamma}\left[1 - \left(\frac{r}{R}\right)^{\gamma}\right] u, \tag{3}$$

where r is the radial direction and R is the section radius. A typical flat velocity profile is adopted with $\gamma = 9$, which corresponds to a momentum correction coefficient of $\alpha = 1.1$. The flat profile assumption has been shown with experimental data that blood velocity profiles, on average, are flat (Sherwin et al., 2003; Alastruey, 2006).

Equations 1 and 2 are closed with a pressure-area relation (or tube law). In this work, the lumen is considered circular and the arterial walls are linear, elastic, and isotropic. Lastly, the vessel wall thickness is assumed negligible relative to the radius (i.e. $h_0 \ll R$), resulting in all external forces being reduced to the circumferential direction. These assumptions result in a tube law of form,

$$p = p_e + \frac{\beta}{A_0}\left(\sqrt{A} - \sqrt{A_0}\right), \qquad \text{where,} \qquad \beta(x) = \frac{E(x)h_0\sqrt{\pi}}{1-\nu^2}, \tag{4}$$

where p_e is the external pressure, A_0 is the area in the reference state, $E(x)$ is the axially-dependent Young's modulus, and ν is the Poisson's ratio.

In the numerical implementation, Equations 1 and 2 are written in conservative form,

$$\frac{\partial \mathbf{U}}{\partial t} + \frac{\partial \mathbf{F}(\mathbf{U})}{\partial x} = \mathbf{S}(\mathbf{U}). \tag{5}$$

2.1.1 Boundary Conditions

The inlet condition will be applied as a flow rate Q, collected via ultrasound in the femoral artery. For non-patient specific simulations, Gaussian waves will be used. To apply the condition, all sources terms in Equation 5, are assumed negligible. Therefore,

$$W_b(A_\star, u_\star) = W_b(A_R, u_R). \tag{6}$$

Arterial networks are created by coupling a single artery to two 'daughter' arteries to create a bifurcation (and vice versa for merging arteries). At these locations, conservation of mass,

$$A_{1\star}u_{1\star} = A_{2\star}u_{2\star} = A_{3\star}u_{3\star}. \tag{7}$$

energy (applied through Bernoulli's law),

$$p(A_{1\star}) + \frac{1}{2}\rho u_{1\star}^2 = p(A_{2\star}) + \frac{1}{2}\rho u_{2\star}^2 \tag{8}$$

$$p(A_{1\star}) + \frac{1}{2}\rho u_{1\star}^2 = p(A_{3\star}) + \frac{1}{2}\rho u_{3\star}^2. \tag{9}$$

and wave characteristics,

$$W_f(A_1, u_1) = W_f(A_{1\star}, u_{1\star}) \tag{10}$$

$$W_b(A_2, u_2) = W_b(A_{2\star}, u_{2\star}) \tag{11}$$

$$W_b(A_3, u_3) = W_b(A_{3\star}, u_{3\star}). \tag{12}$$

(for the case of splitting arteries) is enforced.

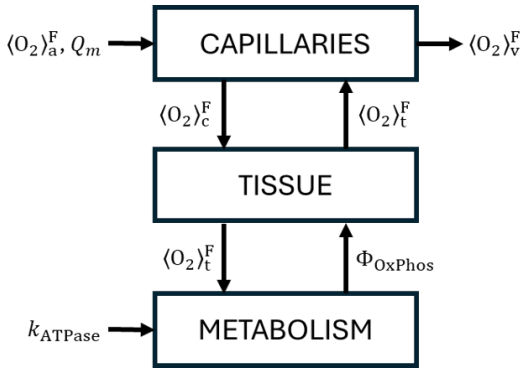

Figure 1: Schematic of the three-compartment mathematical model designed to model oxygen transport and utilisation in skeletal muscle.

For flow past the terminal vessels, lumped Windkessel models are currently used[1]. Windkessel models can take multiple forms; the most common being the three-element resistor-capacitor-resistor (RCR) model. The governing equations taking the form of,

$$C\frac{dp_C}{dt} = q_{in} - q_{out}. \tag{13}$$

Implementation of these models follow the methods presented in Alastruey, K. H. Parker, et al., 2008.

2.2 Skeletal Muscle

Transport of *total* oxygen concentration $\langle O_2 \rangle^T$ is modelled as a three-compartment model (blood b, tissue t, cellular metabolism) based on the work of Lai et al., 2009 and as illustrated in Figure 1. Transport of *free* oxygen in the capillaries (i.e. blood) $\langle O_2 \rangle^F_b$ occurs via advection (driven by blood flow), diffusion (within the blood), and perfusion (into the tissue); described by an advection-diffusion-reaction (ADR) partial differential equation (PDE),

$$f_b \frac{\partial \langle O_2 \rangle^F_b}{\partial t} = Q_m \frac{\partial \langle O_2 \rangle^F_b}{\partial v} + D_b \frac{\partial^2 \langle O_2 \rangle^F_b}{\partial v^2} - \frac{\mathcal{P}}{\gamma_b}\left(\langle O_2 \rangle^F_b - \langle O_2 \rangle^F_t\right), \qquad \text{in } 0 < v < V_m \tag{14}$$

where f_b is the blood volume fraction (of the muscle volume), $Q_m(t)$ is the muscle blood flow (l min^{-1}), D_b is the rate of diffusion in blood (l^2 min^{-1}), $\mathcal{P}(t)$ is the permeability-surface area product (min^{-1}), γ_b describes the chemical equilibrium between *total* to *free* concentration, $\langle O_2 \rangle^F_t$ is the *free* oxygen concentration is the tissue (ml), and V_m is the total muscle volume (l).

In the tissue, a lumped representation of the total $\langle O_2 \rangle^F_t$ and its utilisation via oxidative phosphorylation (OxPhos) is described by an ordinary differential equation (ODE),

$$\frac{d \langle O_2 \rangle^F_t}{dt} = \frac{\mathcal{P}}{\gamma_t V_t} \int_0^{V_m} \left(\langle O_2 \rangle^F_b - \langle O_2 \rangle^F_t\right) \, dv - \frac{\Phi_{OxPhos}}{\gamma_t}, \tag{15}$$

where γ_t is the tissue equivalent to γ_b, V_t is the total tissue volume, and Φ_{OxPhos} is the metabolic flux as part of OxPhos.

For the transport of oxygen, V_m is comprised on the blood and tissue volumes,

$$V_m = V_t + V_b, \tag{16}$$

[1]These will soon be replaced with more detailed models more akin to the work done by Olufsen, 1998. See Section 2.3.

where V_b can be split into the volumes in each vessel type (arteries, capillaries, and venules) so that,

$$V_\mathrm{m} = V_\mathrm{t} + (V_\mathrm{art} + V_\mathrm{cap} + V_\mathrm{ven}). \tag{17}$$

The respective volume fractions f, therefore, add up to 1,

$$1 = f_\mathrm{t} + f_\mathrm{b}. \tag{18}$$

The same applies for the volume fractions of blood ω,

$$1 = \omega_\mathrm{art} + \omega_\mathrm{cap} + \omega_\mathrm{ven}. \tag{19}$$

In this model, the capillary volume is the only variable volume, $V_\mathrm{cap} = V_\mathrm{cap}(t)$ (i.e. the tissue, artery, and venule volumes are constant).

Cellular metabolism is described by a coupled set of ODEs representing the dynamics of adenosine triphosphate (ATP) and phosphocreatine (PCr), including the decomposition of ATP (i.e. production of energy, ATPase) and the production of ATP via OxPhos and the phosphagen system (i.e. ATP + Cr $\rightleftharpoons$ ADP + PCr, where Cr is creatine and ADP is adenosine diphosphate). They are formed as follows,

$$\frac{d\langle \mathrm{ATP}\rangle}{dt} = -\Phi_\mathrm{ATPase} + \beta\Phi_\mathrm{OxPhos} + \Delta\Phi_\mathrm{CK}, \tag{20}$$

$$\frac{d\langle \mathrm{PCr}\rangle}{dt} = \Phi^\mathrm{r}_\mathrm{CK} - \Phi^\mathrm{f}_\mathrm{CK} = -\Delta\Phi_\mathrm{CK}, \tag{21}$$

here, concentrations are represented by $\langle\ \rangle$, metabolic fluxes are represented by Φ, β is the stoichiometric coefficient, $\Phi^{\mathrm{f,r}}_\mathrm{CK}$ are the forward and reverse fluxes that are facilitated by the creatine kinase (CK) enzyme.

Moreover, the metabolic fluxes Φ are functions of the $\langle\mathrm{ATP}\rangle$ and $\langle\mathrm{PCr}\rangle$. The ATPase reaction is linearly proportional to $\langle\mathrm{ATP}\rangle$,

$$\Phi_\mathrm{ATPase} = k_\mathrm{ATPase}\langle \mathrm{ATP}\rangle, \tag{22}$$

where k_ATPase is the ATPase rate constant which depends on exercise intensity. Φ_OxPhos is non-linearly related to both $\langle\mathrm{ADP}\rangle$ and $\langle \mathrm{O_2}\rangle^\mathrm{F}_\mathrm{t}$

$$\Phi_\mathrm{OxPhos} = V_\mathrm{max}\left(\frac{\langle \mathrm{ADP}\rangle}{K_\mathrm{ADP} + \langle \mathrm{ADP}\rangle}\right)\left(\frac{\langle \mathrm{O_2}\rangle^\mathrm{F}_\mathrm{t}}{K_\mathrm{m} + \langle \mathrm{O_2}\rangle^\mathrm{F}_\mathrm{t}}\right), \tag{23}$$

where V_max is the maximal rate of oxidative phosphorylation and both K_ADP and K_m are Michaelis-Menten constants.

$\Delta\Phi_\mathrm{CK}$ is non-linearly related to the concentrations pairs

$$\Delta\Phi_\mathrm{CK} = \Phi^\mathrm{f}_\mathrm{CK} - \Phi^\mathrm{r}_\mathrm{CK} = \frac{\frac{V^\mathrm{f}_\mathrm{CK}}{K_\mathrm{b}K_\mathrm{ia}}\left(\langle \mathrm{ADP}\rangle\langle \mathrm{PCr}\rangle - \frac{\langle \mathrm{Cr}\rangle\langle \mathrm{ATP}\rangle}{K_\mathrm{eq}}\right)}{1 + \frac{\langle \mathrm{ADP}\rangle}{K_\mathrm{ia}} + \frac{\langle \mathrm{ATP}\rangle}{K_\mathrm{iq}} + \frac{\langle \mathrm{PCr}\rangle}{K_\mathrm{ib}} + \frac{\langle \mathrm{ADP}\rangle\langle \mathrm{PCr}\rangle}{K_\mathrm{b}K_\mathrm{ia}} + \frac{\langle \mathrm{Cr}\rangle\langle \mathrm{ATP}\rangle}{K_\mathrm{iq}K_\mathrm{p}}}, \tag{24}$$

where V^f_CK is maximal rate of forward CK reaction and the various K values are all constants, all values used are taken from Lai et al., 2009.

The concentration pairs, ATP-ADP and PCr-Cr, are balanced by mass conservation of adenosine ($\langle \mathrm{Ad}\rangle^\mathrm{T} = 8.2$) and creatine ($\langle \mathrm{Cr}\rangle^\mathrm{T} = 42$), respectively, the totals of which stay constant during moderate exercise, leading to the follow relations

$$\langle \mathrm{Ad}\rangle^\mathrm{T} = \langle \mathrm{ADP}\rangle + \langle \mathrm{ATP}\rangle, \tag{25}$$

$$\langle \mathrm{Cr}\rangle^\mathrm{T} = \langle \mathrm{Cr}\rangle + \langle \mathrm{PCr}\rangle. \tag{26}$$

2.3 Model of Microcirculation

The microcirculation will act as boundary conditions to the macrocirculation. This will be achieved by solving a simplified system of equations for the flow within the arterioles and capillaries; thereby, providing a description of the peripheral resistance. This system will be coupled to the outgoing boundary conditions of the terminal vessels of the macrocirculation. Currently, lumped Windkessel models are providing this information; however, these models do not provide the required information (i.e. shear stress in individual vessels) for describing dilation of the microvasculature. As such, research into alternative approaches is being done. This could take a similar form to what has been presented in Olufsen, 1998; Olufsen, 1999; Steele et al., 2007. These papers use semi-analytical solutions to the linearised 1D Navier–Stokes equations. The most recent of these papers present further developments to include a method of modelling both rest and exercise condition but not the transition between states (which is required for this work).

With knowledge of the flow conditions within the microcirculation and the oxygen kinetics within the skeletal muscle, dilation of the vascular beds can be described. There are two primary pathways to vasodilation that make up functional sympatholysis — a phenomenon where the sympathetic vasoconstriction due to noradrenaline release (at the onset of exercise) is partially inhibited in order to redistribute blood flow to where it is needed (Sinkler et al., 2017). These pathways include,

1. Rapid Onset Vasodilation (ROV),
2. Slow Onset Vasodialtion (SOV).

ROV is mediated by endothelial-derived hyperpolarisation (EDH), whereas SOV is mediated by metabolic activity and shear stress (Sinkler et al., 2017). Research into modelling this processes is still ongoing.

3 Numerical Implementation

The systems described above will be solved using the (legacy) FEniCS computing platform (i.e. an open-source finite element based PDE solver) via the Python library (Logg et al., 2012). All code produced for this project will soon be available on GitHub.

References

Alastruey, Jordi (2006). "Numerical modelling of pulse wave propagation in the cardiovascular system: development, validation and clinical applications". PhD thesis. Imperial College London. URL: https://spiral.imperial.ac.uk/entities/publication/b58717d7-895b-40a3-947f-2453226df8a3.

Alastruey, Jordi, K. H. Parker, et al. (2008). "Lumped parameter outflow models for 1-D blood flow simulations: Effect on pulse waves and parameter estimation". en. In: *ResearchGate*. URL: https://www.researchgate.net/publication/228661502_Lumped_parameter_outflow_models_for_1-D_blood_flow_simulations_Effect_on_pulse_waves_and_parameter_estimation (visited on 04/04/2025).

Alastruey, Jordi, Kim H. Parker, and Spencer J. Sherwin (Oct. 2012). "Arterial pulse wave haemodynamics". In: *11th International Conference on Pressure Surges*. Ed. by S Anderson. Lisbon: Virtual PiE Led t/a BHR Group, pp. 401–443. ISBN: 978-1-85598-133-1.

Fowkes, F Gerald R et al. (Oct. 2013). "Comparison of global estimates of prevalence and risk factors for peripheral artery disease in 2000 and 2010: a systematic review and analysis". In: *The Lancet* 382.9901, pp. 1329–1340. ISSN: 0140-6736. DOI: 10.1016/S0140-6736(13)61249-0. URL: https://www.sciencedirect.com/science/article/pii/S0140673613612490 (visited on 12/14/2024).

Houghton, John S M et al. (June 2024). "New Horizons in Peripheral Artery Disease". In: *Age and Ageing* 53.6, afae114. ISSN: 0002-0729. DOI: 10.1093/ageing/afae114. URL: https://www.ncbi.nlm.nih.gov/pmc/articles/PMC11178507/ (visited on 07/10/2025).

Lai, Nicola et al. (June 2009). "Modeling oxygenation in venous blood and skeletal muscle in response to exercise using near-infrared spectroscopy". In: *Journal of Applied Physiology* 106.6. Publisher: American Physiological Society, pp. 1858–1874. ISSN: 8750-7587. DOI: 10.1152/japplphysiol.91102.2008. URL: https://journals.physiology.org/doi/full/10.1152/japplphysiol.91102.2008 (visited on 10/24/2024).

Logg, Anders, Kent-Andre Mardal, and Garth Wells, eds. (2012). *Automated Solution of Differential Equations by the Finite Element Method: The FEniCS Book*. en. Vol. 84. Lecture Notes in Computational Science and Engineering. Berlin, Heidelberg: Springer. ISBN: 978-3-642-23098-1 978-3-642-23099-8. DOI: 10.1007/978-3-642-23099-8. URL: https://link.springer.com/10.1007/978-3-642-23099-8 (visited on 06/23/2025).

Olufsen, A. S. (1998). "Modeling the arterial system with reference to an anesthesia simulator". PhD thesis. Roskilde: Roskilde Universitet.

— (Jan. 1999). "Structured tree outflow condition for blood flow in larger systemic arteries". In: *American Journal of Physiology-Heart and Circulatory Physiology* 276.1. Publisher: American Physiological Society, H257–H268. ISSN: 0363-6135. DOI: 10.1152/ajpheart.1999.276.1.H257. URL: https://journals.physiology.org/doi/full/10.1152/ajpheart.1999.276.1.h257 (visited on 02/21/2025).

Pabon, Maria et al. (Feb. 2022). "Sex Differences in Peripheral Artery Disease". In: *Circulation Research* 130.4. Publisher: American Heart Association, pp. 496–511. DOI: 10.1161/CIRCRESAHA.121.320702. URL: https://www.ahajournals.org/doi/10.1161/CIRCRESAHA.121.320702 (visited on 08/14/2024).

Sherwin, S. J. et al. (2003). "Computational modelling of 1D blood flow with variable mechanical properties and its application to the simulation of wave propagation in the human arterial system". en. In: *International Journal for Numerical Methods in Fluids* 43.6-7. _eprint: https://onlinelibrary.wiley.com/doi/pdf/10.1002/fld.543, pp. 673–700. ISSN: 1097-0363. DOI: 10.1002/fld.543. URL: https://onlinelibrary.wiley.com/doi/abs/10.1002/fld.543 (visited on 03/19/2025).

Sinkler, Shenghua Y. and Steven S. Segal (2017). "Rapid versus slow ascending vasodilatation: intercellular conduction versus flow-mediated signalling with tetanic versus rhythmic muscle contractions". en. In: *The Journal of Physiology* 595.23. _eprint: https://physoc.onlinelibrary.wiley.com/doi/pdf/10.111 pp. 7149–7165. ISSN: 1469-7793. DOI: 10.1113/JP275186. URL: https://onlinelibrary.wiley.com/doi/abs/10.1113/JP275186 (visited on 07/30/2025).

Sprenger, Lukas et al. (Nov. 2021). "Type 2 diabetes and the risk of cardiovascular events in peripheral artery disease versus coronary artery disease". eng. In: *BMJ open diabetes research & care* 9.2, e002407. ISSN: 2052-4897. DOI: 10.1136/bmjdrc-2021-002407.

Steele, Brooke N., Mette S. Olufsen, and Charles A. Taylor (Feb. 2007). "Fractal network model for simulating abdominal and lower extremity blood flow during resting and exercise conditions". eng. In: *Computer Methods in Biomechanics and Biomedical Engineering* 10.1, pp. 39–51. ISSN: 1025-5842. DOI: 10.1080/10255840601068638.